Spectroscopic Studies of Perturbed T1 Cu Sites in the Multicopper Oxidases *Saccharomyces cerevisiae* Fet3p and *Rhus vernicifera* Laccase: Allosteric Coupling between the T1 and Trinuclear Cu Sites†

Anthony J. Augustine,‡ Mads Emil Kragh,§,‡ Ritimukta Sarangi,‡ Satoshi Fujii,‡ Barry D. Liboiron,‡ Christopher S. Stoj,⊥ Daniel J. Kosman,*,⊥ Keith O. Hodgson,||,‡ Britt Hedman,|| and Edward I. Solomon*,||,‡

Department of Chemistry, Stanford University, Stanford, California 94305, Faculty of Life Sciences, Department of Natural Sciences, University of Copenhagen, Denmark, Stanford Synchrotron Radiation Laboratory, SLAC, Stanford University, Stanford, California 94309, and Department of Biochemistry, School of Medicine and Biomedical Science, State University of New York, Buffalo, New York 14214

Received October 5, 2007; Revised Manuscript Received December 8, 2007

ABSTRACT: The multicopper oxidases catalyze the $4e^-$ reduction of O_2 to H_2O coupled to the $1e^-$ oxidation of 4 equiv of substrate. This activity requires four Cu atoms, including T1, T2, and coupled binuclear T3 sites. The T2 and T3 sites form a trinuclear cluster (TNC) where O_2 is reduced. The T1 is coupled to the TNC through a T1-Cys-His-T3 electron transfer (ET) pathway. In this study the two T3 Cu coordinating His residues which lie in this pathway in Fet3 have been mutated, H483Q, H483C, H485Q, and H485C, to study how perturbation at the TNC impacts the T1 Cu site. Spectroscopic methods, in particular resonance Raman (rR), show that the change from His to Gln to Cys increases the covalency of the T1 Cu−S Cys bond and decreases its redox potential. This study of T1−TNC interactions is then extended to *Rhus vernicifera* laccase where a number of well-defined species including the catalytically relevant native intermediate (NI) can be trapped for spectroscopic study. The T1 Cu−S covalency and potential do not change in these species relative to resting oxidized enzyme, but interestingly the differences in the structure of the TNC in these species do lead to changes in the T1 Cu rR spectrum. This helps to confirm that vibrations in the cysteine side chain of the T1 Cu site and the protein backbone couple to the Cu−S vibration. These changes in the side chain and backbone provide a possible mechanism for regulating intramolecular T1 to TNC ET in NI and partially reduced enzyme forms for efficient turnover.

The multicopper oxidases (MCOs) are an important class of enzymes found in many organisms, including plants, fungi, bacteria, and humans. Well-known members of this class include laccase (Lc) (*1*, *2*), ascorbate oxidase (AO) (*3*), Fet3p (*4*), ceruloplasmin (hCP) (*5*), CueO (*6*), CotA (*7*), and phenoxazinone synthase (*8*). They are important for lignin formation in plants (plant Lc), lignin degradation and detoxification processes in fungi (fungal Lc), and ferroxidase activity in yeast (Fet3p) and humans (hCP) (*9*, *10*). MCOs catalyze four single electron oxidations of a substrate coupled to the four-electron reduction of dioxygen to water (*11*, *12*).

The active site structure of these enzymes (Figure 1) (*13*) is highly conserved and consists of at least four copper atoms, classically divided into three types based upon their different spectral features (*11*). The type 1 (T1) or blue copper site is characterized by an intense Cys-S-to-Cu(II) charge transfer (CT) transition at ∼610 nm and a very small parallel hyperfine coupling in electron paramagnetic resonance (EPR), typically $40-90 \times 10^{-4}$ cm^{-1} (*14*−*16*). The T1 site dominates absorption, circular dichroism (CD), and magnetic circular dichroism (MCD) spectra of the MCOs due to the highly covalent Cu $d_{x^2-y^2}$-Cys Sπ bond (*17*, *18*). It is also the site of substrate oxidation, where the substrate either transfers its electron to the T1 through an outersphere mechanism (Lc, AO) or through a specific substrate binding site and associated protein pathway (Fet3p, hCp). The type

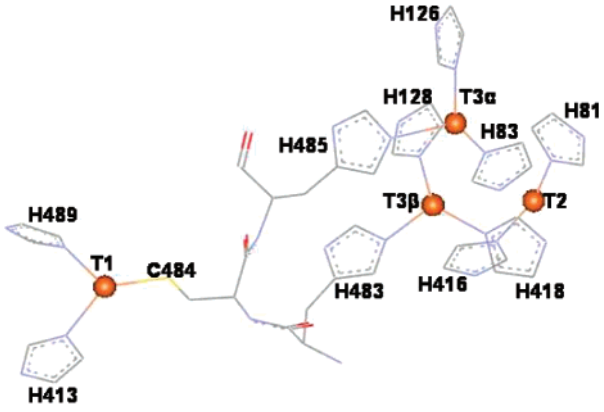

FIGURE 1: Active site structure of Fet3 showing the T1 Cu site, TNC, and the Cys-His pathway which bridges the sites (*13*).

† This research was supported by NIH Grants DK31450 (to E.I.S.), RR-01209 (to K.O.H.), and DK53820 (to D.J.K.).

* To whom correspondence should be addressed. E.I.S.: phone, (650) 723-9104; fax, (650) 725-0259; e-mail, edward.solomon@stanford.edu. D.J.K.: phone, (716) 829-2842; e-mail, camkos@buffalo.edu.

‡ Department of Chemistry, Stanford University.

§ University of Copenhagen.

|| Stanford Synchrotron Radiation Laboratory, SLAC, Stanford University.

⊥ State University of New York.

10.1021/bi7020052 CCC: $40.75
Published on Web 01/16/2008

2 (T2) or normal copper site is characterized by a lack of absorption and CD features, but since it is paramagnetic, it exhibits excited-state features in the low-temperature MCD spectrum. The T2 also has an EPR spectrum with a large parallel hyperfine splitting, $150-200 \times 10^{-4}$ cm^{-1}, typical of planar Cu sites (*16*, *19*, *20*). The type 3 (T3) or coupled binuclear Cu site (*21*) has an intense CT band at 330 nm, originating from an OH^- bridging ligand. The binuclear site exhibits a number of weak ligand field (LF) transitions in the CD spectrum due to the low symmetry at both copper sites; however, no EPR or low-temperature MCD feature is present due to the antiferromagnetic coupling between the two T3 coppers (*19*, *20*). The T2 and T3 sites form a trinuclear cluster (TNC), the existence of which was first demonstrated by spectroscopy (*22*, *23*) and later confirmed in several crystal structures (*24*).

The TNC is the site at which dioxygen is reduced to water (*12*, *25*). When a fully reduced MCO is reacted with O_2, the native intermediate (NI) is formed and can be trapped before it decays to the resting oxidized enzyme (*26*−*28*). NI has been trapped by rapid freeze-quench methods in laccase and has been studied in detail (*29*), as have a number of structurally related model complexes (*30*). In Fet3p, the rates of formation and decay of NI are such that no more than 15% NI can be obtained (A. J. Augustine, L. Quintanar, and E. I. Solomon, unpublished results). These studies have shown that NI is the fully oxidized and catalytically relevant species in the turnover of the MCOs (*11*), the O−O bond has been fully cleaved (*29*), and the oxygen atoms remain bound to the trinuclear cluster as μ_3-oxo and μ_2-hydroxo (between the T3 Cu's) bridges (*31*).

Multiple sequence alignments have confirmed a very high degree of conservation around the active sites in MCOs, including the X−HCH−X motif, which forms a Cys-His bridge between the T1 and T3 (Figure 1) (*11*). This bridge provides an efficient super exchange pathway for rapid intramolecular ET from the T1 Cu to the trinuclear cluster. The T1 Cu redox potentials in the MCOs vary widely, from as low as ∼300 mV (*32*), to as high as ∼800 mV (*33*). This wide range reflects the differences in physiologically relevant substrates among the MCOs. Early studies of *Rhus vernicifera* laccase have shown that the TNC potential is close to that of the T1 site, and a possible allosteric coupling between the two redox sites has been suggested in studies of the holo enzyme, and the deoxy (reduced T3) and met (oxidized T3) type 2 depleted (T2D) derivatives of *Rhus vernicifera* laccase (*34*). Allosteric coupling was suggested based on changes in the T1 resonance Raman (rR) and absorption spectra which occur upon oxidation of the T3 Cu site. Recent studies in *Alcaligenes xylosoxidans* nitrite reductase have indicated small changes in the T1 rR spectra upon binding of nitrite to the T2 Cu site, which is 13 Å away but also bridged by a Cys-His pathway (*34*).

In this study, residue H483, one leg of the Cys-His pathway, has been mutated to generate the H483Q and H483C (Figure 1) mutants in Fet3, and these have been studied in detail to systematically probe the impact of varying the T1-Cys-His-T3 pathway on the spectroscopic features, redox, and electron transfer (ET) properties of the T1 Cu site. Residue H485, the other leg in the Cys-His pathway, was also mutated to create the H485Q and H485C variants, but these were studied in less detail due to their exhibiting additional paramagnetic Cu (more than T1 and T2 sites). This study of the T1−T3 interaction was then extended to catalytically relevant species in *Rhus vernicifera* laccase where the native intermediate can be trapped for spectroscopic study. Furthermore, we evaluate the possible role of the geometric and electronic structure of the TNC in modulating intramolecular ET from the T1 Cu site.

MATERIALS AND METHODS

All chemicals were reagent grade and used without further purification, and water was purified to a resistivity of 15-17 $M\Omega$ cm^{-1} using a Barnsted Nanopure deionizing system. The site-directed mutagenesis was performed, using a QuickChange kit from Stratagene, in the pDY148 vector containing the truncated version of the *FET3* gene. Complementary primers encoding the mutants (H483Q, H483C, H485Q, and H485C) were used in the PCR amplification of the vector. The *FET3* sequences were routinely confirmed by automated fluorescent sequencing at Roswell Park Cancer Institute DNA sequencing Laboratory. The vectors containing WT, H483Q, H483C, H485Q, and H485C were transformed into M2* for soluble protein expression and were isolated and purified according to previously published methods (*36*, *37*).

Rhus vernicifera laccase (*p*-diphenol:dioxygen oxidoreductase) was isolated from acetone powder (Saito & Co, Osaka, Japan) and assayed according to previously published procedures (*33*, *38*). *R.v.* T2D laccase was prepared by chemical removal of the T2 copper, as described in refs 32 and 37. Met T2D was prepared by adding a 15-fold excess of H_2O_2 to deoxy T2D and allowing this to incubate for 30 min. Excess H_2O_2 was removed by buffer exchange before use. Resting oxidized laccase was also treated with excess H_2O_2 to ensure complete oxidation of the T3 copper sites. The native intermediate was prepared using approximately 1.0 mM *R.v.* laccase in 100 mM sodium phosphate pH 7.5 made anaerobic by flushing with argon gas on a Schlenk line for 3 h. Four-electron equivalents of degassed ascorbate were added and allowed to equilibrate for 30 min. The reaction mixture was loaded into a stopped-flow syringe, and the second syringe was loaded with O_2 saturated buffer (1.4 mM at 4 °C). The two syringes were then assembled for rapid mixing with an Update Instruments System 1000 with a Wiskind Grid mixing system. Samples were sprayed directly into liquid nitrogen and packed into 4 mm quartz EPR tubes.

Protein concentrations were determined using the Bradford dye-binding assay (*40*). Copper content was measured spectrophotometrically using a 2,2′-biquinoline assay (*41*). The concentration of paramagnetic copper was detected by spin quantitation of the EPR spectrum using a 1.0 mM aqueous copper standard (1 mM $CuSO_4 \cdot H_2O$ with 2 mM HCl and 2 M $NaclO_4$) (*42*). Absorption spectra were obtained at room temperature (298 K) on a Hewlett-Packard HP8452A or Agilent 8453 diode array UV-visible absorption spectrophotometer. X-band EPR spectra were obtained at 77K with a Bruker EMX spectrometer, ER 051 QR microwave bridge, and ER 4102ST cavity. Samples were measured in 4 mm EPR tubes (quartz) from Wilmad and maintained at 77 K using a liquid N_2 finger dewar with nitrogen gas flow to prevent condensation. EPR simulations were performed using

XSophe (Brüker). Room-temperature CD and low-temperature MCD spectra were measured with a Jasco J-810-150S spectropolarimeter operating with an S-20 photomultiplier in the UV−vis region and a Jasco J-200-D spectropolarimeter using a liquid nitrogen cooled InSB detector for the near IR spectral region. Protein samples were buffer exchanged into 100 mM deuterated potassium phosphate at pD 7.5 and mixed with 50% (v/v) glycerol-d_3, to obtain high quality glasses for MCD. CD spectra were run in a 0.5 cm quartz cuvette. MCD samples were run in cells fitted with two quartz disks and a 3 mm rubber spacer. To subtract any glass-induced baseline shift all samples were run at 7 T, 0 T, and −7 T, and the spectra presented are the subtracted average. Spectra from both instruments were overlaid to cover the entire energy region from 2000-300 nm. Gaussian fitting of MCD spectra was performed using PeakFit 4.0 from Jandel.

RR spectra were obtained on Princeton Instruments ST-135 back-illuminated CCD detector on a Spex 1877 CP triple monochromator with 1200, 1800, and 2400 grooves/mm holographic spectrograph gratings. An Innova 90C Kr^+ laser from Coherent provided the excitation at 647.1 nm. Protein samples, 0.6−1.0 mM, were buffer exchanged into 100 mM sodium phosphate pH 7.5 and measured in 4 mm EPR tubes (quartz) from Wilmad and maintained at 77 K using a liquid N_2 finger dewar. Spectra were obtained using 50 mW laser power with 3 min scans. All spectra presented have been corrected for buffer. Baseline corrections were performed using PeakFit 4.0 (Jandel).

The Cu K-edge X-ray absorption spectroscopic data for the H483Q and H483C Fet3 mutants were measured at the Stanford Synchrotron Radiation Laboratory on the focused 16-pole, 2-T wiggler beam line 9-3 under standard ring conditions of 3 GeV and 85−100 mA. An Si(220) double crystal monochromator was used for energy selection, a Rh-coated collimating pre-monochromator mirror for harmonic rejection, and a cylindrical Rh-coated bent post-monochromator mirror for focusing. The protein samples were prepared as solutions with ∼30% glycerol and loaded into 1 mm Lucite XAS cells with 67 μm Kapton windows. The samples were immediately frozen and stored under liquid nitrogen. The samples were maintained at a constant temperature of ∼10 K during data collection using an Oxford Instruments CF 1208 continuous flow liquid helium cryostat. Data were measured to $k = 9.5$ Å^{-1} in fluorescence mode using a Canberra Ge 30-element array detector. Internal energy calibration was accomplished by simultaneous measurement of the absorption of a Cu-foil placed between two ionization chambers situated after the sample. The first inflection point of the foil spectrum was assigned to 8980.3 eV. Although several scans were collected for each sample, data presented here are the first scans of Fet3 H483Q and H483C to eliminate spectral changes due to photoreduction. The energy-calibrated data were processed by fitting a second-order polynomial to the preedge region, which was subtracted from the entire spectrum as background. A one-region spline of order 2 was used to model the smoothly decaying postedge region background. Normalization of the data was achieved by subtracting the spline and assigning the edge jump to 1.0 at 9000 eV using the *SPLINE* routine in the XFIT suite of programs.

For poised potential measurements, 300 μL of 0.1−0.2 mM Fet3 or laccase in 10 mM potassium phosphate pH = 6.5 were made anaerobic by purging with argon on a Schlenk line. A known concentration of $K_3[Fe(CN)_6]$ was added to the protein solution and titrated with aliquots of an anaerobic solution of $K_4[Fe(CN)_6]$. Equilibrium was achieved after approximately 15 min, and the absorbance at 608 nm was measured under anaerobic conditions. Data were fit to the Nernst equation.

Table 1: Fet3 Copper Quantitation

Fet3 protein	WT	H483Q	H483C
Cu content (Cu/protein)	3.8 ± 0.3	3.9 ± 0.2	3.1 ± 0.2
EPR spin quantitation (spin/protein)	1.8	1.1	1.1
% paramagnetic copper	48%	28%	35%

RESULTS AND ANALYSIS

1.1. Characterization of H483Q and H483C Fet3 Mutants.

Protein yield, copper content, and spin quantitation of recombinant Fet3 protein (WT) are in accordance with previously reported data (Table 1) (*9*). H483Q and H483C mutants were expressed in slightly lower yields in accordance with previous results for inner sphere Fet3 mutants (*20*, *43*). Copper content determination showed that H483Q loads approximately four coppers, while H483C loads approximately three coppers per protein. X-Band EPR spectra of H483Q, shown in Figure 2A (red), and H483C, shown in Figure 2B (green), are significantly different from WT (blue) in that they lack a T2 Cu signal and have a perturbed T1 Cu EPR signal. The EPR spectrum of the T1 Cu site in both mutants will be addressed in section 1.2. Spin quantitation of the EPR spectrum of H483Q shows that there are 1.08 spins/protein, indicating that only one copper center is paramagnetic, which is the T1 site based on the EPR spectrum. Spin quantitation of H483C showed 1.11 spins/protein, which from EPR is also the T1 Cu (Table 1). Thus, all EPR features observed originate from an oxidized T1 Cu site in these mutants.

Cu K-edge XAS experiments were carried out to determine the oxidation states and coordination number of the copper atoms in the TNC in the two mutants. The normalized Cu K-edge XAS data of Fet3 H483C and Fet3 H483Q are compared to those of a fully oxidized MCO in Figure 3. In both H483C and H483Q an intense transition is observed at ∼8983.8 eV which is absent in the spectrum of oxidized MCOs. The rising-edge maxima of H483C and H483Q at 9000 eV are lower in energy and intensity relative to that of an oxidized MCO. Kau et al. showed that the Cu K-edge XAS region of Cu(I) species consists of an intense edge feature at ∼8984 eV corresponding to the Cu 1s → 4p transition (*44*). The intensity and energy of this transition is characteristic of the coordination number of the Cu(I) site. The 8984 eV feature and the rising edge energy shift indicate the presence of reduced Cu in H483C and H483Q. The simulation of the edges of the two mutants included an oxidized T1 site and required a 3:1 contribution of Cu(I):Cu(II) in H483Q and 2:1 for H483C. The best simulation indicates that H483Q contains two 2-coordinate Cu(I), one 3-coordinate Cu(I), and the oxidized T1, while H483C contains one 2-coordinate Cu(I), one 3-coordinate Cu(I), and one oxidized T1 site. The XAS fits are provided in the Supporting Information, Figure S1.

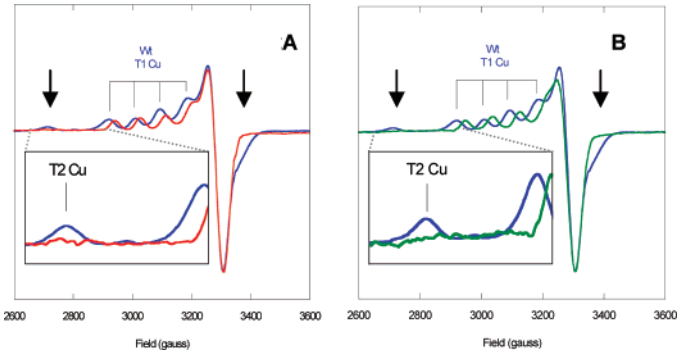

FIGURE 2: A and B: Overlaid EPR spectra; WT is shown in blue, H483Q in red (A), and H483C in green (B). Arrows mark the spectral changes between the mutants and WT in the T2 Cu signal. Inserted in the lower left of both spectra are enlargements of the parallel region where T2 copper EPR typically appears. The characteristic T1 hyperfine splitting is marked for WT in both figures. All spectra were collected at 77 K and 9.522 GHz microwave frequency.

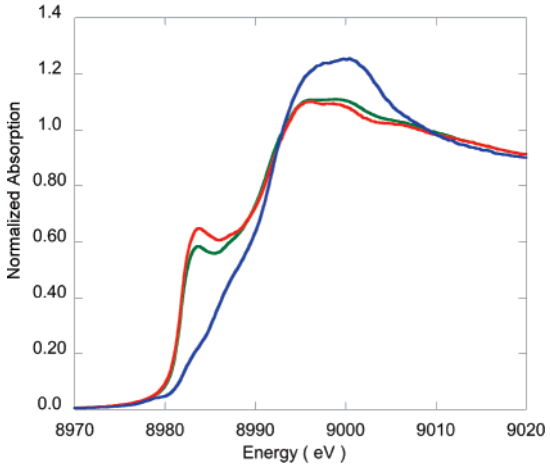

FIGURE 3: The normalized Cu K-edge XAS spectra of oxidized *Rhus vernicifera* laccase in blue, Fet3 H483Q in red, and H483C in green.

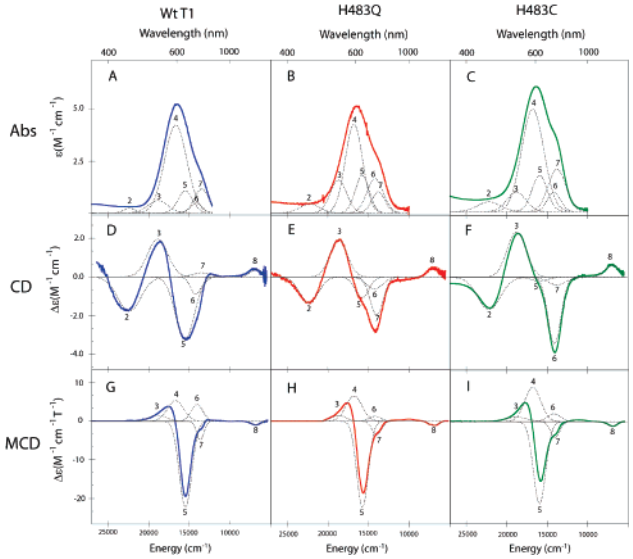

FIGURE 4: A−I: Absorption, CD, and MCD data from Fet3 WT T1 in blue, H483Q in red, and H483C in green. Absorption and CD spectra were obtained at room temperature whereas MCD spectra were obtained at 5 K and 7 T. Spectra of T1 Fet3 WT T1 were generated by subtracting T1D Fet3 data from WT. Band numbers in the figure correspond to band numbers in Table 2.

On the basis of this initial characterization, H483Q loads four coppers with an oxidized T1 Cu and reduced TNC. The XAS indicates that in this reduced TNC there is one 3-coordinate and two 2-coordinate Cu(I). In the case of H483C, which loads three coppers, including an oxidized T1 Cu, XAS revealed that there are two reduced coppers in the cluster and that one is 2-coordinate and one 3-coordinate. Thus for both mutants, only the T1 Cu site contributes to the EPR and absorption (ABS), CD, MCD, and rR spectral features. Furthermore, since the TNC is reduced in the mutants, they do not turnover in the presence of O_2 and substrate.

1.2. Perturbation of the Type 1 Cu in H483Q and H483C.

ABS, CD, and MCD experiments were carried out to probe the spectral features of the T1 Cu in the two mutants. Spectra from these experiments, along with data from the WT T1 site, are shown in Figure 4. The optical spectra for the two mutants appear to be fairly similar in the CT (16 000 − 27 000 cm^{-1}) as well as LF (5000 − 16 000 cm^{-1}) energy regions compared to WT. The ABS, CD, and MCD spectra were simultaneously fit for each species. Bands were numbered according to previous fits for the T1 site in WT Fet3 and plastocyanin (*14*, *45*, *46*). The transition energies obtained from the fits are given in Table 2 and included graphically (dotted Gaussians) in all spectra.

The absorption spectra are given in Figure 4A−C. They are all dominated by an intense feature at 16 500 cm^{-1} (608 nm) the primary component of which is band 4, the Cys-Sπ → Cu (II) $d_{x^2-y^2}$ CT transition. The intensity of this band is found to increase from ϵ = 5500 to 5800 to 7000 M^{-1} cm^{-1} in WT, H483Q, and H483C, respectively. This increase in CT intensity is indicative of an increase in covalency of the Cu−S bond. The intense feature at 16 500 cm^{-1} has a low energy shoulder due to LF transitions of the T1 Cu. These, along with additional CT bands to higher energies, are better resolved in the CD and MCD spectra.

Table 2: Summary of Optical Data from the T1 Site in WT, H483Q and H483C Fet3

		electronic transitions: energy (cm^{-1})			
band	origin	WT T1	H483Q	H483C	*P.p.* laccase[a]
8	d_{z^2}	6800	6950	7000	6900
7	d_{xy}	13500	13900	13900	13300
6	d_{yz}	14100	14200	14200	14400
5	d_{xz}	15400	15600	15750	15900
4	Sπ	16700	16800	16800	16500
3	S pseudo σ	18900	18700	18800	18900
2	Nπ	22400	22300	22200	N/A

[a] Parameters from *P. pinsitus* laccase serves for comparisons.

Table 3: Summary of EPR Data from the T1 Site in WT, H483Q and H483C Fet3

parameter	WT T1	H483Q	H483C	*P.p* laccase[a]
$g_{\|\|}$	2.203	2.185	2.175	2.194
$A_{\|\|}$ ($\times 10^{-4}$ cm^{-1})	88	90	92	90
$g_{\perp}$	2.045	2.045	2.047	2.043
$A_{\perp}$ ($\times 10^{-4}$ cm^{-1})	6	6	6	8

[a] Parameters from *P. pinsitus* laccase serves for comparisons.

CD (4D−F) and MCD (4G−I) spectra allow resolution of the four LF transitions. Band 8, assigned as the $d_{z^2} \rightarrow d_{x^2-y^2}$ transition is found near 7000 cm^{-1} (positive in CD and negative in MCD). The intensity of this transition is similar in the three species; however, it shifts slightly up in energy from WT to H483Q to H483C. The three remaining LF transitions overlap to sum to a negative CD feature at 14 000 cm^{-1} and a negative MCD feature at 15 000 cm^{-1} with a low-energy negative shoulder. The primary change observed for these transitions is in the CD spectra where the intensity and width of the 14 000 cm^{-1} feature varies among the three species. This is due to the fact that the three LF transitions, $d_{xy} \rightarrow d_{yz} \rightarrow$, and $d_{xz} \rightarrow d_{x^2-y^2}$ (bands 7, 6, and 5) are all found to shift slightly up in energy (see Table 2), and the $d_{xy} \rightarrow d_{x^2-y^2}$ (band 7) has switched from positive to negative sign in CD. Minor, but similar, changes can be seen in the 15 000 cm^{-1} negative MCD feature, due to the increase in energy of the three LF transitions. In addition, two features are observed in the CD spectra at 20 000 (+) cm^{-1} and 23 000 (−) cm^{-1} and one feature in the MCD spectrum at 18 000 (+) cm^{-1}. These allow resolution of the Cys S pseudo σ (band 3) and His π (band 2) $\rightarrow d_{x^2-y^2}$ CT transitions, as well as the $S\pi \rightarrow d_{x^2-y^2}$ transition (band 4), which dominates the absorption spectra. While these transitions are found at similar energies in the three species, the four LF transitions all shift up in energy by a few hundred wavenumbers in the mutants. This is again indicative of a destabilization of the $d_{x^2-y^2}$ orbital resulting from an increase in covalency of the Cu−S bond.

The X-band EPR spectra for WT, H83Q, and H483C in Figure 2 were simulated to obtain the spin Hamiltonian parameters for the T1 in Table 3. The most obvious difference is the significant decrease in $g_{||}$ from 2.203 in WT to 2.185 in H483Q and to 2.175 in H483C. Equation 1 gives the LF expression for $g_{||}$, which is dependent upon λ, the spin−orbit coupling parameter for Cu (II), and α^2 and β^2, the amount of metal character in the $d_{x^2-y^2}$ and d_{xy} orbitals, respectively, reflecting the covalency, and E_{xy}-$E_{x^2-y^2}$, the $d_{xy} \rightarrow d_{x^2-y^2}$ transition energy (*47*).

$$g_{||} = 2.00 - \left(\frac{8\lambda\alpha^2\beta^2}{E_{xy} - E_{x^2-y^2}}\right) \quad (1)$$

Thus the $g_{||}$ value is dependent upon the covalency and the $d_{xy} \rightarrow d_{x^2-y^2}$ transition energy. From the simultaneous fit of the ABS, CD, and MCD data, the $d_{xy} \rightarrow d_{x^2-y^2}$ transitions were found to increase by 400 cm^{-1} in the mutants compared to WT. This increase in energy is not large enough to explain the large decrease in $g_{||}$. This indicates that increased covalency of the Cu−S bond must play the primary role in decreasing $g_{||}$. In addition, $A_{||}$ is found to increase slightly from 88 $\times 10^{-4}$ cm^{-1} in WT to 90 $\times 10^{-4}$ cm^{-1} in H483Q and to 92 $\times 10^{-4}$ cm^{-1} in H483C. The increased covalency in the mutants would, in principle, decrease the $A_{||}$ value; however, the *g* values also contribute to the hyperfine through the orbital dipolar coupling term. The decrease in $g_{||}$ due to increased covalency in the mutants is in fact responsible for the increase in magnitude of $A_{||}$ (*48*).

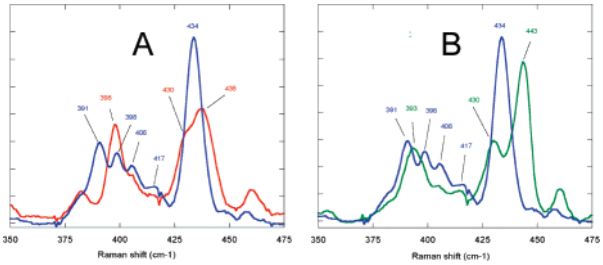

FIGURE 5: Resonance Raman spectra of Fet3 WT in blue with H483Q in red (A) and H483C in green (B) overlaid. RR spectra were obtained upon excitation at 647.1 nm, and at 77 K.

The ABS, CD, MCD, and EPR data have shown that while the structure of the T1 site in H483Q and H483C has not changed significantly, these mutations at T3β Cu in the TNC have increased the covalency of the T1 Cu−S bond, 13 Å away, as seen by the increase in intensity of the $S\pi \rightarrow$ Cu $d_{x^2-y^2}$ CT transition in the ABS, the slightly increased LF strength in CD and MCD, and the decrease of $g_{||}$ in EPR.

1.3. Resonance Raman Spectroscopy and Poised Potentials.

A number of resonance enhanced vibrations are observed around 400 cm^{-1} upon laser excitation into the T1 $S\pi \rightarrow$ Cu $d_{x^2-y^2}$ CT band (band 4, Figure 4). These vibrations have been shown to have predominantly Cu−S stretching character. The fact that these vibrational modes occur at comparable frequencies in all blue copper sites is in further support of their highly conserved geometric structures and ground states.

The rR spectrum for Fet3 WT is shown in blue and overlaid with H483Q in red (Figure 5A) and H483C in green (Figure 5B). The WT rR spectrum is dominated by an intense peak at 434 cm^{-1} and a number of less intense peaks between 391 and 417 cm^{-1}. The rR spectra of H483Q and H483C exhibit a number of vibrational transitions in the same region as WT; however, significant differences are observed. In H483Q, the intense peak around 434 cm^{-1} has broadened, containing two resolvable bands, one at 438 cm^{-1} and a shoulder at 430 cm^{-1}. A similar but more significant effect can be seen in H483C, with the intense peak at 443 cm^{-1} and a shoulder at 430 cm^{-1}. The less intense peaks in the two mutants are also present at similar energies as in WT, but their intensities differ as does the number of resolved peaks. Thus, the rR spectra of the T1 Cu site in WT, H483Q, and H483C all exhibit one intense peak around 435 cm^{-1}, clearly shifting up in energy from WT to H483Q to H483C. This peak is dominated by the Cu−S stretch distortion, based on its dominant resonance intensity in the S → Cu CT transition, and its frequency increases with an increase in the covalency of the Cu−S bond (*49*).

In blue copper sites the Cu−S stretch is distributed over several mixed modes (*vide infra*), so the intensity-weighted average vibrational energy is used to determine the strength of the Cu−S bond (*50*). The fits to the rR spectra of the three species are shown in Supporting Information, Figure S2. From these, intensity-weighted average frequencies are WT $\langle \upsilon_{Cu-S} \rangle = 415$ cm^{-1}, H483Q $\langle \upsilon_{Cu-S} \rangle = 419$ cm^{-1}, and

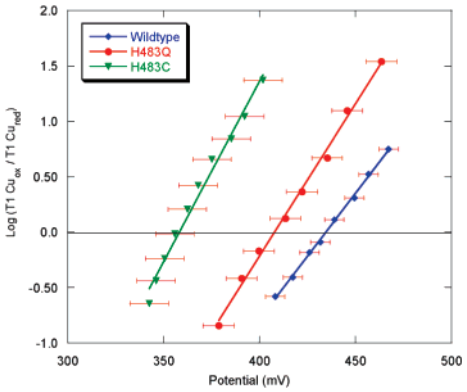

FIGURE 6: Poised Potential titration of Type 1 Cu site in Fet3 WT, H483Q, and H483C. Solid line is best fit for three sets of data to the Nernst equation.

Table 4: Summary of Intensity Weighted Average Frequencies and T1 Cu Redox Potential

Fet3 protein	$\langle \upsilon_{Cu-S} \rangle$ (cm^{-1})	$E°$ (mV)
WT	415.0	434 ± 5
H483Q	419	408 ± 8
H483C	423	359 ± 10

H483C $\langle \upsilon_{Cu-S} \rangle = 423$ cm^{-1}. These frequencies are in good accord with the rR results for other MCOs which lack an axial ligand, e.g., *P.p.* Lc, $\langle \upsilon_{Cu-S} \rangle = 413$ cm^{-1}, and *P.v.* Lc, $\langle \upsilon_{Cu-S} \rangle = 421$ cm^{-1} (*49*, *50*). The increase in intensity-weighted average frequency indicates that a stronger Cu−S bond is present in the mutants compared to WT which by Badger's Rule (*51*) corresponds to a ∼1% decrease in bond length in H483C relative to WT. This is also reflected in a more stabilized Cu(II) redox state of the T1 site in the mutants compared to WT. Figure 6 shows the results of poised potential titrations of WT, H483Q, and H483C. There is a significant lowering of the T1 redox potential for the variants relative to WT. Reduction potentials were determined to be 434 ± 5 mV in WT, 408 ± 8 mV in H483Q, and 359 ± 10 mV in H483C.

To summarize, these rR data along with the optical and EPR data, support a model where the T1 Cu−S bond increases in covalency as the T3β Cu has one of its ligands, residue 483, mutated from His to Gln to Cys. This increase in covalency contributes to a decrease in redox potential of the T1 Cu as summarized in Table 4.

1.4. Characterization of H485Q and H485C Fet3 Mutants.

Residue H485, the other leg in the T1 Cu-Cys-His-T3 Cu ET pathway, was also mutated to generate the H485Q and H485C mutants. Initial characterization (Supporting Information, Table S1) showed that while H485Q has ∼4 Cu/protein and ∼2 spins/protein, the EPR spectrum (Supporting Information, Figure S4) is complicated. showing the presence of more paramagnetic species than the usual T1 and T2 Cu sites. H485C is also complicated in that it shows >4 Cu/protein and >3 spins/protein. In both of these mutants, the presence of extra paramagnetic species complicated further spectroscopic studies, i.e., CD and MCD. However, the absorption spectrum of the mutants (Supporting Information, Figure S3) is still dominated by the T1 S$\pi \rightarrow$ Cu $d_{x^2-y^2}$ CT band which makes it possible to directly probe the Cu−S bond independent of the other Cu in the protein through rR spectroscopy (Figure 7). These experiments show a similar trend, with an

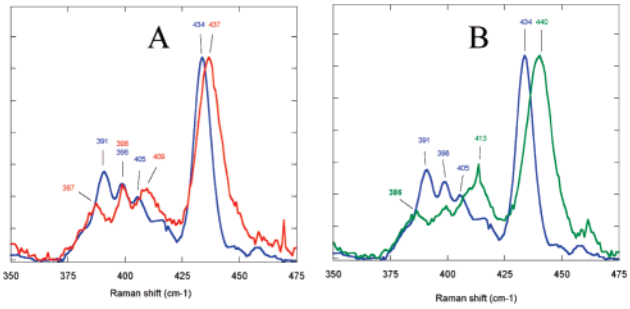

FIGURE 7: Resonance Raman spectra of Fet3 WT in blue with H485Q in red (A), and H485C in green (B) overlaid. RR spectra were obtained upon excitation at 647.1 nm^{-1}, and at 77 K.

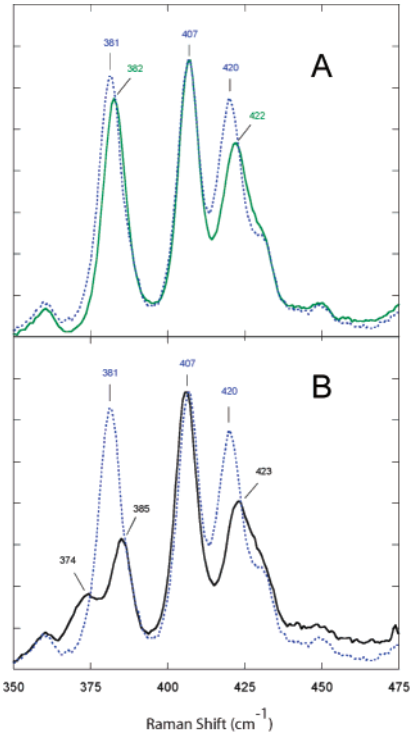

FIGURE 8: Resonance Raman profiles of met T2D in blue with Rest. Ox. Lc. in green (A) and deoxy T2D in black (B) overlaid. RR spectra were obtained upon excitation at 647.1 nm, and at 77 K.

increase in $\langle \upsilon_{Cu-S} \rangle$ from WT, 415 cm^{-1}, to H485Q, 421 cm^{-1}, to H485C, 424 cm^{-1}.

1.5. T1−T3 Interactions in *Rhus vernicifera* Laccase.

To gain insight into the T1-trinuclear interaction in catalytically relevant species, rR experiments were carried out on NI and derivatives of holo *R.v.* laccase including deoxy and met T2D (where T2D has the T2 Cu depleted and deoxy has T3 Cu's reduced, while in met, T3 is oxidized). These studies were conducted on *R.v.* laccase where the native intermediate can be trapped in high yield for rR spectroscopic study.

The presence of an axial methionine ligand at the T1 site in laccase weakens the Cys S−Cu bond; thus, the intense vibrational features in its rR spectrum are shifted down in energy relative to Fet3p and other three coordinate blue copper sites (*45*, *49*). Figure 8A shows the rR spectrum of Rest. Ox. Lc. overlaid with that of met T2D. The rR spectra of the two species are very similar with three intense features around ∼380, 407, and ∼420 cm^{-1} and weaker peaks at 360 and 430 cm^{-1}. The similarity between these indicates

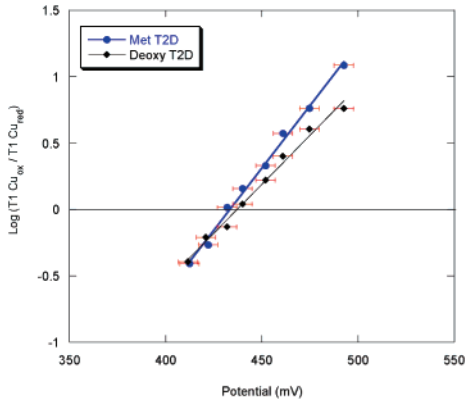

FIGURE 9: Poised potential titration of met and deoxy T2D. Solid line is best fit for two sets of data to the Nernst equation.

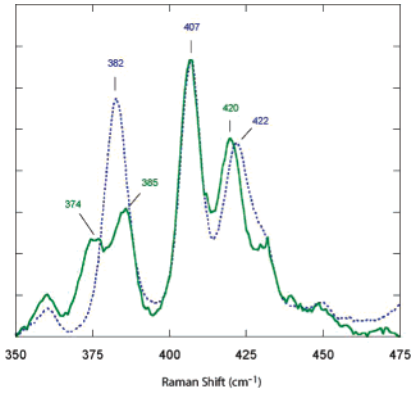

FIGURE 10: Resonance Raman profiles of Rest. Ox. Lc. in blue overlaid with NI Lc. in green. RR spectra were obtained upon excitation at 647.1 nm, and at 77 K.

minimal structural differences in the Cu−S bond at the T1 site. Figure 8B shows rR spectra of deoxy T2D overlaid with met T2D (absorption spectra shown in Supporting Information, Figure S6). Deoxy T2D has two intense peaks at 407, and 423 cm^{-1}, and weaker features at 360, 374, and 385 cm^{-1}. The splitting of the intense features in the ∼380 cm^{-1} region of deoxy T2D suggests that there are at least two vibrations contributing in this region. As described above, the intensity weighted average frequencies for Rest. Ox. Lc., met T2D, and deoxy T2D were used to estimate the strength of the Cu−S bond. Average energies for all three species were found to be the same within error, $\langle \upsilon_{Cu-S} \rangle = 404 \pm 1$ cm^{-1}. Poised potential titrations were carried out for met T2D and deoxy T2D, using the $[Fe(CN)_6]^{3-}/[Fe(CN)_6]^{2-}$ redox couple, and both species were found to have $E°$ of 433 ± 5 mV (Figure 9). The reduction potential for the T1 site in resting oxidized *R.v.* laccase has been determined by several groups to be 430−440 mV (*33*, *52*).

Figure 10 presents the rR spectrum of NI Lc. (confirmed by EPR, Supporting Information, Figure S7) overlaid with that of Rest. Ox. Lc. (taken from Figure 8A). The spectrum of NI Lc. is dominated by two intense vibrations at 407 and 420 cm^{-1}, with weaker peaks at 360, 374, 385, and ∼430 cm^{-1}. Intensity-weighted average frequencies of the two species were Rest. Ox. Lc. $\langle \upsilon_{Cu-S} \rangle = 404$ cm^{-1} and NI Lc. $\langle \upsilon_{Cu-S} \rangle = 403$ cm^{-1}, which are the same within experimental resolution. Although no T1 redox potential measurement could be conducted for NI Lc. because of its decay, the intensity weighted average vibrational energy indicates that the Cu−S bond in NI Lc. is not perturbed relative to Rest. Ox. Lc.

Importantly, the two weaker peaks at ∼374 and 385 cm^{-1} in the NI Lc. rR spectrum in Figure 10 reflect a splitting of the ∼380 cm^{-1} vibrational feature of Rest. Ox. Lc. This is very similar to the splitting observed in this energy region of the deoxy T2D spectrum relative to the met T2D spectrum (Figure 8B). This strongly suggests that the origin of this splitting may be similar in deoxy T2D and NI Lc. As met and deoxy T2D and Rest. Ox. Lc. show no measurable difference in redox potential or average frequency, the changes observed in the 380 cm^{-1} region of deoxy T2D (Figure 8B) likely also do not reflect a difference in the Cu−S bond but rather a change in vibrational modes coupling with the Cu−S vibration. This appears to also be the case for NI Lc.

DISCUSSION

The goal of this study was to evaluate T1-TNC interactions in the MCOs by site directed mutagenesis of the T1-Cys-His-T3 pathway in Fet3, and relate the findings to well-defined catalytically relevant species in *Rhus vernicifera* laccase. All four Fet3 mutants in this study targeted ligands at the TNC; however, in all mutants a perturbation of the T1 site, which is >13 Å away, was observed. The perturbation at the T1 increased the covalency of the Cu−S bond, thus lowering the T1 Cu redox potential, as the T3α-H483-C484 or T3β-H485-C484 interactions were perturbed by mutating these residues from His to Gln, which interacts with the T3 Cu more weakly than His, and then to Cys, which apparently is too short to interact with the T3 Cu.

From the complementary spectroscopic data on the Gln mutant, the TNC is present but reduced and the Gln-Cu(I) interaction is weak (i.e., XAS showed two of the reduced Cu's to be 2-coordinate) while in the Cys mutant one T3 Cu is missing. ABS, CD, and MCD spectra of the T1 in WT, H483Q, and H483C showed very similar CT and LF transition energies, indicating very similar T1 Cu sites in the three species. However, the increase in absorption intensity (band 4 Figure 4A−C) and lowering of the $g_{||}$ value in the EPR spectrum (Figure 2A and 2B) indicate that these mutations of a T3 ligand have led to an increase in covalency of the T1 Cu−S bond.

The rR spectrum provides a direct probe of the strength/covalency of the Cu−S bond. In the H483 mutants the high-intensity vibration (∼434 cm^{-1} in WT) is shifted up in energy and the intensity-weighted average energy is increased indicative of an increase in Cys S−Cu bond strength. Redox potential measurements carried out on these mutants showed that as the strength of the Cu−S bond increased, the reduction potential decreased.

All the findings in Fet3 mutants suggest a mechanical model, where weakening or elongating the bond to a T3 Cu relaxes the T1 Cu-Cys-His-T3 Cu backbone and allows better overlap between the Cu $d_{x^2-y^2}$ and Cys Sπ orbitals, creating a more covalent bond to the T1 Cu. The thiolate donates more charge, thus stabilizing the Cu(II) relative to the Cu(I) state as reflected in the lower reduction potentials for the mutants.

In contrast to the results for the Fet3 mutants, no observable change in the Cu−S bond was detected by rR

spectroscopy in the four laccase species studied: Rest. Ox. Lc., NI Lc., met T2D, and deoxy T2D. These results suggest that while all four species have very different electronic and geometric structures of the trinuclear (and binuclear for T2D) cluster, the T1 Cu redox potential is not significantly affected. There is no difference in the intensity weighted average energy of the Cu−S vibration in any of the four species, and as the redox potentials of met T2D, deoxy T2D, and Rest. Ox. Lc. did not significantly change, it is likely that NI Lc. also has a similar redox potential (∼430 mV). This is interesting, as an altered redox potential at the T1 Cu in NI Lc. or deoxy T2D compared to Rest. Ox. Lc. would provide a regulation mechanism for selective reduction.

The similarity in the rR spectra between Rest. Ox. Lc. and met T2D (Figure 8A) suggests a very similar geometric and electronic structure of the T1 Cu. The small change in the 420 cm^{-1} region indicates that the presence of the T2 does have a limited effect on the T1 vibrations. However, in contrast to met T2D, the rR spectrum of deoxy T2D showed two resolved vibrations in the ∼380 cm^{-1} region, and differences between the two species are also notable around 420 cm^{-1}. Interestingly two vibrations are also observed around ∼380 cm^{-1} in the rR spectrum of NI Lc (Figure 10); however, the features in the ∼420 cm^{-1} region are more similar to Rest. Ox. Lc.

The fact that the rR spectra of NI Lc. and deoxy T2D exhibit two vibrations around ∼380 cm^{-1} with very similar frequencies strongly suggests that they reflect a similar vibrational mode coupling to the Cu−S vibration. Furthermore, this change in vibrational energy relative to Rest. Ox. Lc. indicates a change in this mode coupling with the Cu−S vibration as a result of a change in the structure of the TNC. The number and types of modes coupling with the Cu−S vibration around 400 cm^{-1} has been the subject of much discussion (*53*−*57*). However, the current consensus is that the primary source of coupling is movement of the protein backbone skeleton near the T1 Cu site (*53*) and more specifically vibration of the Sγ−C$_\beta$−C$_\alpha$−N unit of the cysteine residue coordinated to the T1 Cu (*54*), with the degree of mixing with the Cu−S stretch increasing as the Cu−Sγ−C$_\beta$−C$_\alpha$ dihedral angle approaches 180°. The axial methionine and histidine ligands are not thought to contribute in this region. The change in the 380 cm^{-1} region of the rR spectra of met T2D versus deoxy T2D and NI Lc coupled with the fact that the Cu−S bond strength does not change in any of these helps to confirm the assignment of these rR features as backbone modes coupling to the Cu−S stretch.

Perturbations of the protein backbone in the vicinity of the T1 Cu site in deoxy T2D and NI Lc. could provide a mechanism for regulating the cysteine backbone carbonyl oxygen atom in its hydrogen bonding to the imidazole ring of a His coordinated to the T3β Cu (dotted black line in Figure 11). This H-bond shunt could provide an additional pathway for ET to the TNC, which can be regulated. The hydrogen bond along the T1-Cys-His-T3 pathway would bypass three carbon and nitrogen atoms and could also significantly effect ET through both constructive and destructive interference (*58*). Given that the distance from the carbonyl oxygen of the Cys residue to the δN of the imidazole ring is only 2.88 Å (*24*), small changes in its length, on the order of 0.1 Å, could significantly impact H_{DA} optimizing the Cys-His pathway to contribute to the rapid ET in NI Lc. to ensure rapid turnover and prevent decay of NI to Rest. Ox. Lc. Also such a structural change can regulate and selectively reduce partially reduced sites to maximize enzyme efficiency under substrate-limited conditions.

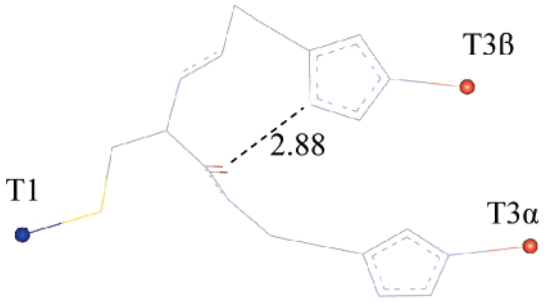

FIGURE 11: Crystal structure of the Cys-His pathway connecting the T1 Cu to the T3 Cu's in ascorbate oxidase (*22*). The dotted line shows the hydrogen bond shunt.

The results of this study suggest that while perturbations of the T3 site can alter the redox potential of the T1 Cu, as in the H483 mutants of Fet3, the redox potential of the T1 Cu does not appear to be allosterically controlled by the redox states of the trinuclear cluster in Lc. However, rR data do show changes in the T1 Cys side chain and backbone vibrations coupled to changes in the redox state and coordination of the trinuclear cluster. Changes in the angles in the cysteine backbone can change the distance and orientation of the hydrogen bond between the cysteine backbone carbonyl and a T3 histidine imidazole ring. This could modulate the electronic coupling between the T1 Cu and the trinuclear cluster and increase the rate of ET in catalytically relevant intermediates and partially reduced species.

ACKNOWLEDGMENT

We would like to thank Dr. Jungjoo Yoon for assistance in resonance Raman spectroscopy and for discussions regarding MCO structures. This research was supported by NIH Grants DK31450 (to E.I.S.), RR-01209 (to K.O.H.), and DK53820 (to D.J.K.). SSRL operations are funded by the Department of Energy, Office of Basic Energy Sciences. The SSRL Structural Molecular Biology program is supported by the National Institutes of Health, National Center for Research Resources, Biomedical Technology Program, and by the Department of Energy, Office of Biological and Environmental Research. A.J.A. is a John Stauffer Stanford Graduate Fellow.

SUPPORTING INFORMATION AVAILABLE

Cu K-edge XAS and rR fits for H483Q and H483C mutants, copper quantitation, absorption, and EPR spectra, redox potential measurements for H485Q and H485C mutants, and absorption spectra of deoxy and met T2D Lc. This material is available free of charge via the Internet at http://pubs.acs.org.

REFERENCES

1. Nitta, K., Kataoka, K., and Sakurai, T. (2002) Primary structure of a Japanese lacquer tree laccase as a prototype enzyme of multicopper oxidases, *J. Inorg. Biochem. 91*, 125−131.
2. Jonsson, L., Sjostrom, K., Haggstrom, I., and Nyman, P. O. (1995) Characterization of a laccase gene from the white-rot fungus

Trametes versicolor and structural features of basidiomycete laccases, *Biochim. Biophys. Acta 1251*, 210−215.
3. Messerschmidt, A., Rossi, A., Ladenstein, R., Huber, R., Bolognesi, M., Guiseppina, G., Marchesini, A., Petruzzelli, R., and Finazzi-Agro, A. (1989) X-ray crystal structure of the blue oxidase ascorbate oxidase from zucchini. Analysis of the polypeptide fold and model of the copper sites and ligands, *J. Mol. Biol. 206*, 513−529.
4. de Silva, D., Askwith, C. C., Eide, D., and Kaplan, J. (1995) The FET3 gene product required for high affinity iron transport in yeast is a cell surface ferroxidase, *J. Biol. Chem. 270*, 1098−1101.
5. Zaitseva, I., Zaitsev, V., Card, G., Moshkov, K., Bax, B., Ralph, A., and Lindley, P. (1996) The X-ray structure of human ceruloplasmin at 3.1 Å: Nature of the copper centres, *J. Biol. Inorg. Chem. 1*, 15−23.
6. Roberts, S., Weichsel, A., Grass, G., Thakali, K., Hazzard, J., Tollin, G., Rensing, C., and Montfort, W. (2002) Crystal structure and electron-transfer kinetics of CueO, a multicopper oxidase required for copper homeostasis in *Escherichia coli*, *Proc. Natl. Acad. Sci. U.S.A. 99*, 2766−2771.
7. Bento, I., Martins, L. O., Lopes, G. G., Carrondo, M. A., and Lindley, P. F. (2005) Dioxygen reduction by multi-copper oxidases; a structural perspective, *Dalton Trans.* 3507−3513.
8. Smith, A. W., Camara-Artigas, A., Wang, M. T., Allen, J. P., and Francisco, W. A. (2006) Structure of phenoxazinone synthase from Streptomyces antibioticus reveals a new type 2 copper center, *Biochemistry 45*, 4378−4387.
9. Quintanar, L., Gebhard, M., Wang, T. P., Kosman, D. J., and Solomon, E. I. (2004) Ferrous binding to the multicopper oxidases *Saccharomyces cerevisiae* Fet3p and human ceruloplasmin: Contributions to ferroxidase activity, *J. Am. Chem. Soc. 126*, 6579−6589.
10. Stoj, C., Augustine, A. J., Zeigler, L., Solomon, E. I., and Kosman, D. J. (2006) Structural Basis of the Ferrous Iron Specificity of the Yeast Ferroxidase, Fet3p, *Biochemistry 45*, 12741−12749.
11. Solomon, E. I., Sundaram, U. M., and Machonkin, T. E. (1996) Multicopper oxidases and oxygenases, *Chem. Rev. 96*, 2563−2605.
12. Messerschmidt, A. (1997) *Multi-Copper Oxidases*, World Scientific Publishing Co., River Edge, NJ.
13. Taylor, A. B., Stoj, C. S., Ziegler, L., Kosman, D. J., and Hart, P. J. (2005) The copper-iron connection in biology: Structure of the metallo-oxidase Fet3p, *Proc. Natl. Acad. Sci. U.S.A. 102*, 15459−15464.
14. Gewirth, A. A., and Solomon, E. I. (1988) Electronic structure of plastocyanin: excited state spectral features, *J. Am. Chem. Soc. 110*, 3811−3819.
15. Solomon, E. I., Penfield, K. W., Gewirth, A. A., Lowery, M. D., Shadle, S. E., Guckert, J. A., and LaCroix, L. B. (1996) Electronic structure of the oxidized and reduced blue copper sites: contributions to the electron transfer pathway, reduction potential, and geometry, *Inorg. Chim. Acta 243*, 67−78.
16. Malmstrom, B. G., Reinhammar, B., and Vanngard, T. (1969) The State of Copper in Stellacyanin and Laccase from the Lacquer Tree Rhus Vernicifera, *Biochim. Biophys. Acta 205*, 48−57.
17. LaCroix, L. B., Shadle, S. E., Wang, Y., Averill, B. A., Hedman, B., Hodgson, K. O., and Solomon, E. I. (1996) Electronic Structure of the Perturbed Blue Copper Site in Nitrite Reductase: Spectroscopic Properties, Bonding, and Implications for the Entatic/Rack State, *J. Am. Chem. Soc. 118*, 7775−7768.
18. LaCroix, L. B., Randall, D. W., Nersissian, A. M., Hoitink, C. W.G., Canters, G. W., Valentine, J. S., and Solomon, E. I. (1998) Spectroscopic and Geometric Variations in Perturbed Blue Copper Centers: Electronic Structures of Stellacyanin and Cucumber Basic Protein, *J. Am. Chem. Soc. 120*, 9621−9631.
19. Cole, J. L., Clark, P. A., and Solomon, E. I. (1990) Spectroscopic and chemical studies of the laccase trinuclear copper active site: geometric and electronic structure, *J. Am. Chem. Soc. 112*, 9534−9548.
20. Palmer, A. E., Quintanar, L., Severance, S., Wang, T.-P., Kosman, D. J., and Solomon, E. I. (2002) Spectroscopic characterization and O_2 reactivity of the trinuclear Cu cluster of mutants of the multicopper oxidase Fet3p, *Biochemistry 41*, 6438−6448.
21. Malkin, R.; Malmström, B.G. (1970) The State and Function of Copper in Biological Systems, *Adv. Enzymol. 33*, 177−243.
22. Allendorf, M. D., Spira, D. J., and Solomon, E. I. (1985) Low temperature MCD studies of native laccase: spectroscopic evidence for exogenous ligand bridging at a trinuclear copper active site, *Proc. Natl. Acad. Sci. U.S.A. 82*, 3063.
23. Spira-Solomon, D. J., Allendorf, M. D., and Solomon, E. I. (1986) Low-temperature magnetic circular dichroism studies of native laccase: confirmation of a trinuclear copper active site, *J. Am. Chem. Soc. 108*, 5318.
24. Messerschmidt, A., Ladenstein, R., Huber, R., Bolognesi, M., Avigliano, L., Petruzzelli, R., Rossi, A., and Finazzi-Agro, A. (1992) Refined crystal structure of ascorbate oxidase at 1.9 Å resolution, *J. Mol. Biol. 224*, 179−205.
25. Cole, J. L., Tan, G. O., Yang, E. K., Hodgson, K. O., and Solomon, E. I. (1990) Reactivity of the laccase trinuclear copper active site with dioxygen: an X-ray absorption edge study, *J. Am. Chem. Soc. 112*, 2243−2249.
26. Solomon, E. I., Chen, P., Metz, M., Lee, S.-K., and Palmer, A. E. (2001) Oxygen binding, activation, and reduction to water by copper proteins, *Angew. Chem., Int. Ed. 40*, 4570−4590.
27. Andréasson, L.-E., and Reinhammar, B. (1976) Kinetic studies of *Rhus vernicifera* laccase. role of the metal centers in electron transfer, *Biochim. Biophys. Acta 445*, 579−597.
28. Andréasson, L.-E., Brändén, R., and Reinhammar, B. (1976) Kinetic studies of *Rhus vernicifera* laccase: evidence for multielectron transfer and an oxygen intermediate in the reoxidation reaction, *Biochim. Biophys. Acta 438*, 370−379.
29. Lee, S. K., George, S. D., Antholine, W. E., Hedman, B., Hodgson, K. O., and Solomon, E. I. (2002) Nature of the intermediate formed in the reduction of O_2 to H_2O at the trinuclear copper cluster active site in native laccase, *J. Am. Chem. Soc. 124*, 6180−6193.
30. Yoon, J., Mirica, L. M., Stack, T. D. P., and Solomon, E. I. (2005) Variable-Temperature, Variable-Field Magnetic Circular Dichroism Studies of Tris-Hydroxy- and μ_3-Oxo-Bridged Trinuclear Cu(II) Complexes: Evaluation of Proposed Structures of the Native Intermediate of the Multicopper Oxidases, *J. Am. Chem. Soc. 127*, 13680−13693.
31. Yoon, J., Liboiron, B. D., Sarangi, R., Hodgson, K. O., Hedman, B., and Solomon, E. I. (2007) The two oxidized forms of the trinuclear Cu cluster in the multicopper oxidases and mechanism for the decay of the native intermediate, *Proc. Natl. Acad. Sci. U.S.A. 104*, 13609−13614.
32. Mondovi, B.; Avigliano, L. (1984) *Ascorbate Oxidase* (Mondovi, B.; Avigliano, L., Eds.) Vol. 3, pp 101−118, CRC Press, Boca Raton, FL.
33. Reinhammar, B. R. (1972) Oxidation-reduction potentials of the electron acceptors in laccases and stellacyanin, *Biochim. Biophys. Acta 275*, 245−259.
34. LuBien, C. D., Winkler, M. E., Thamann, T. J., Scott, R. A., Co, M. S., Hodgson, K. O., and Solomon, E. I. (1981) Chemical and spectroscopic properties of the binuclear copper active site in Rhus laccase: direct confirmation of a reduced binuclear type 3 copper site in type 2 depleted laccase and intramolecular coupling of the type 3 to the type 1 and type 2 copper sites, *J. Am. Chem. Soc. 103*, 7014−7016.
35. Kohzuma, T., Kikuchi, M., Horikoshi, N., Nagatomo, S., Kitagawa, T., and Czernuszewicz, R. S. (2006) Intersite Structural Rearrangement of the Blue Copper Site Induced by Substrate Binding: Spectroscopic Studies of a Copper-Containing Nitrite Reductase from *Alcaligenes xylosoxidans* NCIMB 11015, *Inorg. Chem. 45*, 8474−8476.
36. Hassett, R. F., Yuan, D. S., and Kosman, D. J. (1998) Spectral and kinetic properties of the Fet3 protein from *Saccharomyces cerevisiae*, a multinuclear copper ferroxidase enzyme, *J. Biol. Chem. 273*, 23274−23282.
37. Askwith, C., Eide, D., Van Ho, A., Bernard, P. S., Li, L., Davis-Kaplan, S., Sipe, D. M., and Kaplan, J. (1994) The *FET3* gene of *S. cerevisiae* encodes a multicopper oxidase required for ferrous iron uptake, *Cell 76*, 403−410.
38. Reinhammer, B. (1970) Purification and Properties of laccase and stellacyanin from *Rhus Vernicifera*, *Biochim. Biophys. Acta 205*, 35−47.
39. Gaziani, M. T., Morpurgo, L., Rotilio, G., and Mondovi, B. (1976) Selective removal of type 2 copper from Rhus vernicifera laccase, *FEBS Lett. 70*, 87−90.
40. Bradford, M. M. (1976) A rapid and sensitive method for the quantitation of microgram quantities of protein utilizing the principle of protein-dye binding, *Anal. Biochem. 72*, 248−254.
41. Felsenfeld, G. (1960) The determination of cuprous ion in copper proteins, *Arch. Biochem. Biophys. 87*, 247−251.
42. Carithers, R. P., and Palmer, G. (1981) Characterization of the potentiometric behavior of soluble cytochrome-oxidase by mag-

netic circular dichroism: evidence in support of heme-heme interaction, *J. Biol. Chem. 256*, 7967−7976.
43. Blackburn, N. J., Ralle, M., Hassell, R., and Kosman, D. J. (2000) Spectroscopic Analysis of the Trinuclear Cluster in the Fet3 Protein from Yeast, a Multinuclear Copper Oxidase, *Biochemistry 39*, 2316−2324.
44. Kau, L. S., Spira-Solomon, D. J., Penner-Hahn, J. E., Hodgson, K. O., and Solomon, E. I. (1987) X-ray absorption edge determination of the oxidation state and coordination number of copper. Application to the type 3 site in Rhus vernicifera laccase and its reaction with oxygen, *J. Am. Chem. Soc. 109*, 6433−6442.
45. Machonkin, T. E., Quintanar, L., Palmer, A. E., Hassett, R., Severance, S., Kosman, D. J., and Solomon, E. I. (2001) Spectroscopy and reactivity of the type 1 copper site in Fet3p from *Saccharomyces cerevisiae*: Correlation of structure with reactivity in the multicopper oxidases, *J. Am. Chem. Soc. 123*, 5507−5517.
46. Kosman, D. J., Hassett, R., Yuan, D. S., and McCracken, J. (1998) Spectroscopic characterization of the Cu(II) Sites in the Fet3 protein, the multinuclear copper oxidase from yeast required for high-affinity iron uptake, *J. Am. Chem. Soc. 120*, 4037−4038.
47. McGarvey, B. R. (1996) in *Transition Metal Chemistry* (Carlin, B. L., Ed.) Vol. 3, pp 89−201.
48. The orbital dipolar term is positive, while the Fermi Contact and spin dipolar terms are negative and dominate $A_{\|}$.
49. Palmer, A. E., Randall, D. W., Xu, F., and Solomon, E. I. (1999) Spectroscopic Studies and Electronic Structure Description of the High Potential Type 1 Copper Site in Fungal Laccase: Insight into the Effect of the Axial Ligand, *J. Am. Chem. Soc. 121*, 7138−7149.
50. Blair, D. F., Campbell, G. W., Schoonover, J. R., Chan, S. I., Gray, H. B., Malmstrom, B. G., Pecht, I., Swanson, B. I., Woodruff, W. H., Cho, W. K., English, A. M., Fry, H. A., Lum, V., and Norton, K. A. (1985) Resonance Raman studies of blue copper proteins: effects of temperature and isotopic substitutions. Structural and thermodynamic implications, *J. Am. Chem. Soc. 107*, 5755−5766.
51. Badger, R. M. (1934) A Relation Between Internuclear Distances and Bond Force Constants, *J. Chem. Phys. 2*, 128−131.
52. Reinhammer, B. R. M., and Vanngard, T. I. (1971) The Electron-Accepting Sites in Rhus vernicifera Laccase as Studied by Anaerobic Oxidation-Reduction Titrations, *Eur. J. Biochem. 18*, 463−468.
53. Urushiyama, A., and Tobari, J. (1990) Resonance Raman Active Vibrations of Blue Copper Proteins. Normal Coordinate Analysis on 169-Atom Model, *Bull. Chem. Soc. Jpn. 63*, 1563−1571.
54. Dave, B. C., Germanas, J. P., and Czernuszewicz, R. S. (1993) The first direct evidence for copper(II)-cysteine vibrations in blue copper proteins: resonance Raman spectra of 34S-Cys-labeled azurins reveal correlation of copper-sulfur stretching frequency with metal site geometry, *J. Am. Chem. Soc. 115*, 12175−12176.
55. Qiu, D., Dong, S., Ybe, J. A., Hecht, M. H., and Spiro, T. G. (1995) Variations in the Type I Copper Protein Coordination Group: Resonance Raman Spectrum of ^{34}S-, ^{65}Cu-, and ^{15}N-Labeled Plastocyanin, *J. Am. Chem. Soc. 117*, 6443−6446.
56. Dong, S., and Spiro, T. G. (1998) Ground- and Excited State Mapping of Plastocyanin from Resonance Raman Spectra of Isotope-Labeled Proteins, *J. Am. Chem. Soc. 120*, 10434−10440.
57. Dong, S., Ybe, J. A., Hecht, M. H., and Spiro, T. G. (1999) H-Bonding Maintains the Active Site of Type 1 Copper Proteins: Site Directed Mutagenesis of Asn38 in *Poplar Plostocyanin*, *Biochemistry 38*, 3379−3385.
58. Balabin, I. A., and Onuchic, J. N. (2000) Dynamically controlled protein tunneling paths in photosynthetic reaction centers, *Science 290*, 114−117.

BI7020052